IEEE Transactions on Industry Applications

Design Trade-off Between Torque Density and Power Factor in Surface-Mounted PM Vernier Machines Through Closed-Form Per-Unit Equations

Yu Zhao, Dawei Li, *Senior Member*, *IEEE*, Xiang Ren, Tianjie Zou, and Ronghai Qu, *Fellow*, *IEEE*

***Abstract*—Benefited from flux modulation effects, surface-mounted permanent magnet vernier machines (SPMVMs) present the high-torque low-speed properties, which can become the potential candidates for direct-drive applications. However, their power factor is inferior to conventional PM machines due to the large inductance caused by parasitic no-working harmonics. This paper is devoted to propose some design considerations of SPMVMs to make a good compromise between torque density and power factor. Via constructing closed-from per-unit equations, the cross-coupling influences of slot/pole combinations and normalized geometric variables on machine performances are revealed. It is found that there is a tradeoff between torque density and power factor. The high magnet thickness to air-gap length ratio is beneficial to decrease inductance, while the flux modulation effect under the large equivalent air-gap length would be impaired. Moreover, the pole-pair ratio, i.e., the PM pole-pair to armature winding pole-pair, should be carefully selected, where the SPMVMs with high pole-pair ratio have the relatively high magnetic loading owing to the strong flux modulation effects, whereas they suffer from the low power factor due to serious harmonic leakage inductance. In particular, taking the end-winding length into consideration, the high torque advantages of high pole-pair ratio SPMVMs under the same copper losses can be well performed with high length-radius ratio. Combined with the analysis, the preferable selections of critical parameters to satisfy various technical indexes are determined. Then, the general design approach is proposed, and two design examples are built and compared. Meanwhile, finite element analysis (FEA) and prototype experiments are carried out to verify the feasibility.**

***Index Terms*—Surface-mounted permanent magnet vernier machines (SPMVMs), pole-pair ratio, normalized parameters, torque density, and power factor.**

I. INTRODUCTION

DIRECT-DRIVE motors have received increasing more attention for wind power generation, marine proportion, and in-wheel tractions. They have the advantages of high efficiency, small vibration noise, and high reliability due to the cancellation of mechanical gear boxes. However, there is still the challenges to overcome considering the high torque density requirements.

Benefited from flux modulation effects, permanent magnet vernier machines (PMVMs) present the low-speed high-torque properties, which can become the promising candidates for direct-drive applications [1-3]. However, PMVMs suffer from low power factor due to the parasitic harmonic inductances, which would increase the volume and cost of inverter [4], [5]. To promote the industrial applications of PMVMs, many researches have been done, which can be classified into two aspects.

1) *Enhancing torque density*. Based on the three elements of PMVMs, i.e., flux modulator, PM excitation, and armature winding, a lot of efforts have been presented to further improve the torque density of PMVMs. In [6] and [7], hybrid tooth surface-mounted permanent magnet vernier machines (SPMVM) has been proposed to enhance the flux modulation effects by introducing multiple working permeance harmonics. Further, interior PM and halbach PM have been applied to strengthen PM flux focusing effects [8], [9]. Alternate rotor flux bridges have been designed to resolve the flux barrier effects occurred in spoke-array PM rotor structure [10], [11]. Moreover, toroidal winding and split tooth concentrated winding structure have been used to reduce the end-winding length [12], [13]. Although the torque density of these topologies mentioned above has been enhanced, the low power factor issues are still existed.

2) *Improving power factor*. The dual-stator spoke-array PM vernier machine has been investigated in [14], where the power factor can be significantly improved by increasing the excitation capability. Further, the dual-side PM structure has been proposed in [15], [16] where the stator and rotor PMs work together to decrease flux leakage. Moreover, the hybrid excitation PMVM has been put forward to enhance the excitation magnetic fields and improve power factor [17]. Nevertheless, these topologies equipped with dual-stator, dual-PM, or dual-excitation, are relatively complex, which are not suitable for the direct-drive applications.

Manuscript received September 1, 2022; revised December 28, 2022; accepted February 12, 2023. Paper 2022-EMC-0983.R1, presented at the 2022 International Power Electronics Conference (IPEC-2022-ECCE-Asia), Himeji, Japan, May. 15–29, and approved for publication in the IEEE TRANSACTIONS ON INDUSTRY APPLICATIONS by the Electric Machines Committee of the IEEE Industry Applications Society. This work was supported by National Natural Science Foundation of China under Grant 51977094, 52122705 and 51991382. (*Corresponding author: Dawei Li*)

Yu Zhao, Dawei Li, Xiang Ren, and Ronghai Qu are with School of Electrical and Electronic Engineering, Huazhong University of Science and Technology, Wuhan 430074, China (e-mail: yuzhao@hust.edu.cn; daweili@hust.edu.cn; renxiang_1993@hust.edu.cn; ronghaiqu@hust.edu.cn).

Tianjie Zou is with the Power Electronics, Machines and Control (PEMC) Group, University of Nottingham, Nottingham NG7 2RD, U.K. (e-mail: Tianjie.Zou@nottingham.ac.uk).

Therefore, it is necessary to investigate more attractive PMVMs with simple structure and low cost for direct-drive applications. Especially, it is found in [18] and [19] that SPMVM with low pole-pair ratio (*PR*), i.e., the pole-pair ratio of PM to armature winding, performs a better power factor characteristic owing to the small parasitic harmonic inductances. Although the average torque of low *PR* SPMVMs are inferior to high *PR* counterparts, the low *PR* SPMVMs endowed with short end-windings are promising for small length-radius ratio conditions [20]. However, current researches are confined to specific size and power rating. There is a lack of the comprehensive analysis and design of SPMVMs to balance average torque and power factor, covering different length-radius ratios and power ratings.

This paper proposes some design considerations of SPMVMs for direct-drive applications, which is devoted to make a good compromise between torque density, power factor, and efficiency, covering different power ratings. According to construct the closed-form per-unit equations, the cross-coupling influences of critical parameters, including pole-pair ratio *PR*, magnet thickness to air-gap length ratio k_g, stator slot opening width to slot pitch ratio k_s, et al, on machine performances are investigated. And the preferable selection ranges of critical parameters are determined. Further, the general design approach of SPMVMs for direct-drive applications are presented, which can avoid the blind attempt and provide a good guidance for engineering designers.

The main contents are organized as follows: First, the closed-from per-unit equations, including magnetic loading *B*, electric loading *A*, normalized inductance *L*, torque density *σ*, and power factor *PF*, are derived in Section II, where the negative correlations between torque and power factor are revealed. Second, Section III deeply investigates the influence of critical parameters, such as pole-pair ratio *PR*, magnet thickness to air-gap length ratio k_g, stator slot opening width ratio k_s, and length-radius ratio k_{shape}, on machine performance. Moreover, the preferable selection ranges are determined. Then, Section IV propose the general design approach for SPMVMs. And the detailed design examples and Finite element analysis (FEA) are given in Section V. Section VI presents the conclusions.

II. Relations Between Torque Density and Power Factor

In this Section, the closed-from per-unit equations of torque density and power factor are constructed, where magnetic loading, electrical loading, and normalized inductance work as the bridges to reveal the negative correlations between torque density and power factor.

To have a clear presentation, all the design parameters are summarized in Table I. And the dimension parameter model of SPMVM is depicted in Fig. 1.

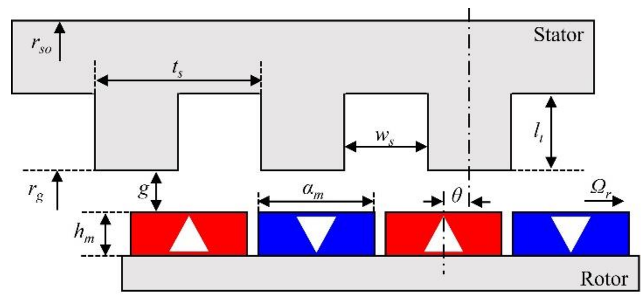

Fig. 1. The dimension parameter model of SPMVM.

TABLE I
DESIGN PARAMETERS OF SPMVMS

Design Parameters	Symbols	Design Parameters	Symbols
Stator slot number	Z_s	The base for inductance normalization	L_{base}
PM pole-pair number	P_r	Normalized total inductance	L
Armature winding pole-pair number	P_a	Normalized main inductance	L_m
Stator outer radius	r_{so}	Normalized harmonic leakage inductance	L_σ
Stator inner radius	r_g	Back-electromotive force	E
Air-gap length	g	Series turns per phase	N_s
Stack length	l_{st}	Phase current RMS value	I
Stator slot pitch	t_s	Rotor position and time	θ, t
Stator slot opening width	w_s	Vacuum permeability and relative permeability	μ_0, μ_r,
Stator slot depth	l_t	PM fundamental MMF	F_{r1}
PM pole-arc	α_m	PM resistance	R_m
PM thickness	h_m	PM remanence	B_r
Average torque	T	Copper resistivity	ρ
Torque density	σ	The ratio of PM pole-pair to armature winding pole-pair	PR
Power factor	PF	Copper loss per-unit volume	k_{Copper}
Efficiency	η	The ratio of PM thickness h_m to air-gap length g	k_g
Slot filling factor	k_f	The ratio of stator slot opening width w_s to stator slot pitch t_s	k_s
Magnetic loading	B	The ratio of stator inner radius r_g to stator outer radius r_{so}	k_{split}
Electric loading	A	The ratio of stack length l_{st} to stator outer radius r_{so}	k_{shape}
Air-Gap relative constant permeance	Λ_0	The ratio of slot depth l_t to stator depth ($r_{so} - r_g$)	k_t
Air-Gap relative fundamental permeance	Λ_1	The ratio of air-gap length g to stator outer radius r_{so}	k_P
P_r^{th} and $(Z_s \pm P_r)^{th}$ MMF harmonic amplitudes	F_{Pr}, $F_{Zs\pm Pr}$	The ratio of total winding length to stack length l_{st}	k_{end}
P_r^{th} and $(Z_s \pm P_r)^{th}$ flux density harmonic amplitudes	B_{Pr}, $B_{Zs\pm Pr}$	Rotor mechanical angular speed	Ω
Winding factors of $(iZ_s \pm P_r)^{th}$ harmonic	$k_{wiZs\pm Pr}$	Rotor electrical angular speed	ω

A. Magnetic Loading

According to magnetomotive force (MMF)-permeance model, no-loading air-gap flux density in SPMVMs is defined as the product of air-gap MMF and permeance [1].

$$\begin{aligned} B(\theta,t) &= F_r(\theta,t) * \Lambda(\theta) \\ &= F_{r1}\cos(P_r\theta-\omega t)(\Lambda_0+\Lambda_1\cos(Z_s\theta)) \\ &= B_{Pr}\cos(P_r\theta-\omega t)+B_{Pr\pm Zs}\cos((P_r\pm Z_s)\theta\mp\omega t) \end{aligned} \tag{1}$$

$$B_{Pr} = k_B \frac{\Lambda_0}{1+\frac{\mu_r}{k_g}} \tag{2}$$

$$B_{Pr\pm Zs} = k_B \frac{\Lambda_1}{2(1+\frac{\mu_r}{k_g})} \tag{3}$$

$$k_g = \frac{h_{\mathrm{m}}}{g},\ k_B = \frac{4}{\pi}B_r(\sin\frac{\alpha_m\pi}{2}) \tag{4}$$

where k_B is the factor that quantifies air-gap harmonics. Λ_0 and Λ_1 are constant and fundamental relative permeance, where the detailed expressions are given in Appendix. Both the Λ_0 and Λ_1 are the function of magnet thickness to air-gap length ratio k_g, and stator slot opening width ratio k_s.

It can be noticed that SPMVMs exist multiple no-load air-gap harmonics having different pole-pairs. And it has been confirmed in [12] that all the air-gap harmonics are working harmonics, which can contribute back-EMF and average torque. Combined with expression of back-EMF and winding function [14], the contribution of each harmonic can be determined.

Further, magnetic loading B of SPMVMs can be given as [7]:

$$\begin{aligned} B &= f(PR,k_s,k_g,P_a,k_w) \\ &= k_{wPr}B_{Pr}+PRk_{wPr-Zs}B_{Pr-Zs}+\frac{PR}{2PR+1}k_{wPr+Zs}B_{Pr+Zs} \end{aligned} \tag{5}$$

where k_w is winding factor of air-gap working harmonics, which has taken account of slot opening factor [2].

It can be found that magnetic loading B of SPMVMs is related to multiple parameters, including pole-pair ratio PR, magnet thickness to air-gap length ratio k_g, stator slot opening width ratio k_s, armature winding pole-pair P_a, and winding factor k_w.

B. Electric Loading

To make a fair comparison, end-winding length and the corresponding copper losses caused by which are taken into consideration. In particular, the copper loss factor k_{Copper}, i.e., the copper losses per-unit volume, is set as a benchmark to reflect machine dissipation capability. Further, electric loading A can be defined as [21]:

$$\begin{aligned} A &= f(PR,k_{shape},P_a,k_t,k_{split},k_s) \\ &= \frac{mN_sI}{\pi r_g} = \sqrt{\frac{k_{Copper}k_fk_tr_{so}^2(1-k_{split})(2k_{split}k_s+k_t(1-k_{split}))}{2\pi\rho k_{end}}} \end{aligned} \tag{6}$$

$$k_{end} = 1+\frac{\pi((2-k_t)k_{split}+k_t)}{(1+PR)P_ak_{shape}}\left\lceil\frac{\lceil PR\rceil}{2}\right\rceil \tag{7}$$

$$k_t = \frac{l_t}{r_{so}(1-k_{split})},\ k_{shape} = \frac{l_{st}}{r_{so}} \tag{8}$$

It can be noticed that electric loading A is related to multiple parameters. Among which, pole-pair ratio PR and length-radius ratio k_{shape} have a significant influence on end-winding length factor k_{end}, which are treated as the most critical parameters for electric loading A. Moreover, electric loading A is also related to stator slot opening width ratio k_s, slot depth ratio k_t, and split ratio k_{split}.

C. Inductance

Different from regular PM machines, the constraints of equal pole-pair between armature winding and PM have been broken in SPMVMs. As a result, the definition of inductance components is also changed. From armature magnetic field perspective, only the armature harmonic which has the same pole-pair P_r of PM, can interact with PM rotor and generate torque. As a result, the normalized main inductance L_m of SPMVMs is defined as the flux linkage produced by the P_r^{th} armature harmonics under per-unit current. Whereas the normalized harmonic leakage inductance L_σ is produced by other no-working armature harmonics, where P_a^{th} armature harmonics are the main components. Slot leakage inductances and end-winding leakage inductances are neglected due to the relatively small proportion.

Then, the inductance L of SPMVMs can be given as [2]:

$$\begin{aligned} L &= f(PR,P_a,k_g,k_{spilt},k_w) \\ &= L_m+L_\sigma \end{aligned} \tag{9}$$

$$L_m = \frac{k_{split}}{k_PP_a}\frac{1}{1+\frac{k_g}{\mu_{\mathrm{r}}}}\left(\frac{k_{wPa}k_{wPr}}{2}\Lambda_1+\frac{k_{wPr}^2}{PR}\Lambda_0\right) \tag{10}$$

$$L_\sigma = \frac{k_{split}}{k_PP_a}\frac{1}{1+\frac{k_g}{\mu_{\mathrm{r}}}}\left(PR*k_{wPa}^2\Lambda_0+\frac{k_{wPa}k_{wPr}}{2}\Lambda_1\right) \tag{11}$$

$$L_{base} = \frac{2\mu_0mN_s^2}{\pi PR*P_a} \tag{12}$$

It can be observed that the inductance is mainly determined by pole-pair ratio PR, armature winding pole-pair P_a, magnet thickness to air-gap length ratio k_g, and winding factor k_w.

D.Torque Density and Power Factor

Combined with magnetic loading B, electric loading A, and inductance L, both the torque density and power factor can be acquired. First, the total volume torque density of SPMVMs can be given as:

$$\sigma = \frac{T}{V_{total}} = \frac{AB\pi r_g^2}{\pi r_{so}^2k_{end}} = \frac{k_{split}^2}{k_{end}}AB \tag{13}$$

Further, under I_d = 0 control and neglecting winding resistance, as shown in Fig. 2, the power factor of SPMVMs can be written as:

$$PF = \frac{E}{\sqrt{E^2+(\omega IL)^2}} = 1\Big/\sqrt{1+(\sqrt{2}\mu_0L\frac{A}{B})^2} \tag{14}$$

This article has been accepted for publication in IEEE Transactions on Industry Applications. This is the author's version which has not been fully edited and content may change prior to final publication. Citation information: DOI 10.1109/TIA.2023.3245586

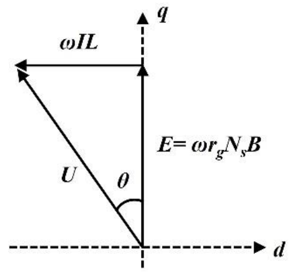

Fig. 2. The vector diagram of SPMVMs under I_d = 0 control.

It can be seen that torque density σ is proportional to the product of k_{split}^2AB/k_{end}, while power factor PF is inversely proportional to LA/B. That is, by selecting magnetic loading B, electric loading A, and inductance L as bridges, the negative correlation between torque density and power factor is revealed. Moreover, they are mutually restricted due to the cross-coupling influence of geometric parameters on which. Thus, there is a trade-off for the design of SPMVMs.

III. Cross-Coupling Influence of Parameters on Machine Performance

Based on the analysis mentioned above, torque density of SPMVMs is negatively correlated with power factor. To make a good compromise between which, the cross-coupling influence of critical parameters, including magnet thickness to air-gap length ratio k_g, stator slot opening width ratio k_s, pole-pair ratio PR, armature winding pole-pair P_a, and length-radius ratio k_{shape}, on machine performance are comprehensively investigated. The detailed analysis is given in what follows, where the variation of machine performances with design parameters are acquired by the analytical calculation equations.

To better reveal the influences of critical parameters on machine performances, six models with different slot/pole combinations are selected for comparisons, covering different pole-pair ratios PR and armature winding pole-pairs P_a. Among which, the model with PR=1, P_a=2 is the regular PM synchronous machine (PMSM) having the same pole-pair of armature winding and PM, which is worked as the benchmark. It can also be treated as the special SPMVM, where the flux modulation effect is weakest [7]. While other models have the different pole-pairs between armature windings and PMs, where the higher pole-pair ratio PR, the stronger flux modulation effects. It is worth noting that the models under different pole-pair ratios have the different coil pitches and end-winding lengths. As a result, under the same copper loss, the models with low PR and compact end-winding can acquire the high active phase current. However, the models with high PR suffer from the low active phase currents. Especially, the selected model with PR=3.5, P_a=2 can have a better balance between flux modulation effects and end-winding lengths.

Table II presents the original design parameters of the six models. To have a fair comparison, all the models have the same stator outer radiuses, air-gap lengths, stack lengths, series turns per phase, total copper losses, and so on. Moreover, the stator inner radiuses, split ratios and stator slot depths are flexibly adjusted to acquire the similar no-load yoke flux density. Although the models under different stator inner radiuses, split ratios and stator slot depths have the different electromagnetic performances, the variation tendencies of performances with targeted parameters are kept unchangeable. To avoid the interference of other parameters on machine performances, the variable control method is applied. That is, only the investigated single variable is changeable, while other parameters are kept invariable.

A. Magnet Thickness to Air-Gap Length Ratio k_g

Fig. 3 shows the influence of magnet thickness to air-gap length ratio k_g on torque density σ and power factor PF, respectively. For regular PMSM, only B_{Pr} and L_m are the main components of air-gap flux density and inductance, while the modulated harmonics $B_{Pr\pm Zs}$ and harmonic leakage inductance L_σ are barely existed. As a result, it can be seen that with the increase of k_g, both the torque density σ and power factor PF of regular PMSM are enhanced due to the increase of magnetic loading B and decrease of inductance, as shown in Fig. 4.

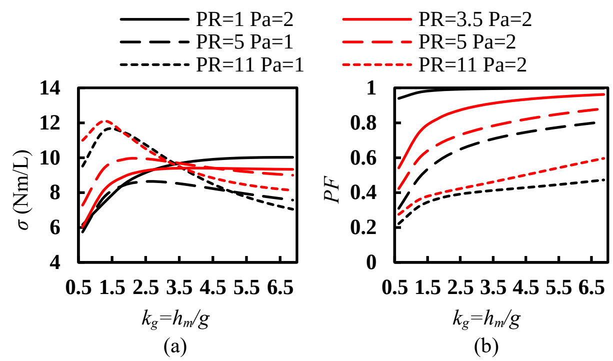

Fig. 3. The influence of magnet thickness to air-gap length ratio k_g. (a) Torque density σ. (b) Power factor PF.

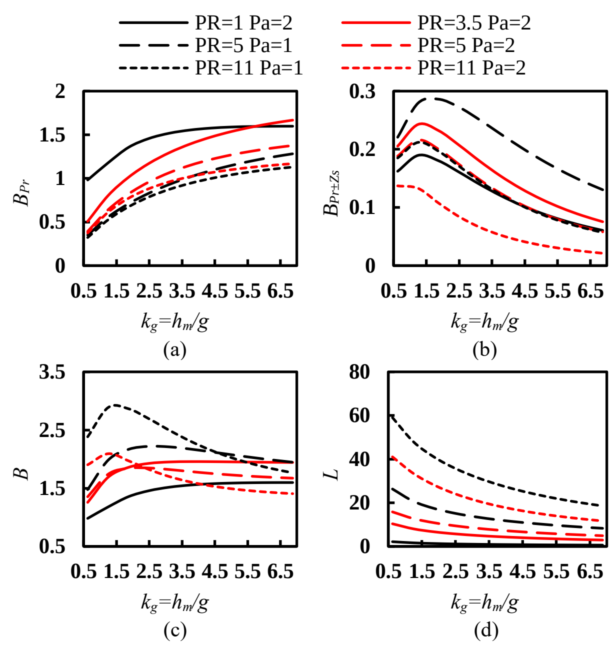

Fig. 4. The influence of magnet thickness to air-gap length ratio k_g. (a) Air-gap harmonic B_{Pr}. (b) Air-gap harmonic $B_{Pr\pm Zs}$. (c) Magnetic loading B. (d) Inductance L.

For SPMVMs, the power factor can also be improved by the increase of k_g, due to the reduction of inductance. While the influences of k_g on torque density σ are more complicated due to there are multiple air-gap working harmonics. On the one hand, increasing k_g, that is, increasing magnet consumption, is beneficial to enhance harmonic B_{Pr}, as shown in Fig. 4(a). On the other hand, the flux modulation effects are deteriorated due to the relatively large equivalent air-gap length. It can be noticed in Fig. 4(b) that the modulated harmonics $B_{Pr\pm Zs}$ are increased first and then dropped due to the decrease of air-gap relative fundamental permeance Λ_1. Thus, with the increase of k_g, the torque density σ of SPMVMs is increased first and then reduced. Under the optimal k_g, the torque density σ of SPMVMs with high pole-pair ratio PR, can be up to several times of regular PMSMs.

Therefore, the selection of k_g can be concluded that:

1) In terms of torque density σ, the optimal k_g of SPMVMs with the same PR is similar. With the increase of PR, the optimal k_g is decreased to strengthen flux modulation effects, as listed in Table I and II.

2) In terms of power factor PF, the relatively large k_g is preferable due to the weakened inductance.

B. Stator Slot Opening Width to Slot Pitch Ratio k_s

Further, the cross-coupling influences of stator slot opening width to slot pitch ratio k_s on torque density σ and power factor PF are investigated, as shown in Fig. 5. With the increase of k_s, the harmonics B_{Pr} is gradually decreased due to the impaired air-gap relative constant permeance Λ_0, as shown in Fig. 6(a). Whereas there is the optimal k_s about 0.6 to acquire the maximum modulated harmonics $B_{Pr\pm Zs}$, as shown in Fig. 6(b). As a result, it can be noticed in Fig .6(c) that magnetic loading B increases first and then reduces. Moreover, Fig. 6(d) and (e) show that with the increase of k_s, the electric loading A under the same copper losses can be improved due to the enlarged slot area. While inductance L is decreased, where the harmonics leakage L_σ is the main components.

On the whole, the effects of k_s on torque density σ is in accordance with magnetic loading B, which climbs up and then declines. However, the effects of k_s on PF are relatively weak, due to the variation of electric loading A and inductance L with k_s are inverse.

The selection of k_s can be concluded that:

1) For torque density σ, the optimal k_s of SPMVMs with the same PR is nearly kept identical, which is around 0.4~0.7. With the increase of PR, the optimal k_s is slightly enlarged to strengthen the contribution of modulated harmonics, as shown in Table I and II.

2) In terms of power factor PF, the influence of k_s on which is relatively weak, which can be neglected.

C.Pole-Pair Ratio PR and Length-Radius Ratio k_{shape}

Combined with the analysis mentioned above, both the selections of k_g and k_s are strongly associated with the selection of pole-pair ratio PR. Thus, for the design of SPMVMs, it is necessary to determine PR at first. The effects of PR on torque density σ and power factor PF are explored under the same copper loss factor k_{Copper} = 76 kW/m^3, covering different length-radius ratio k_{shape}.

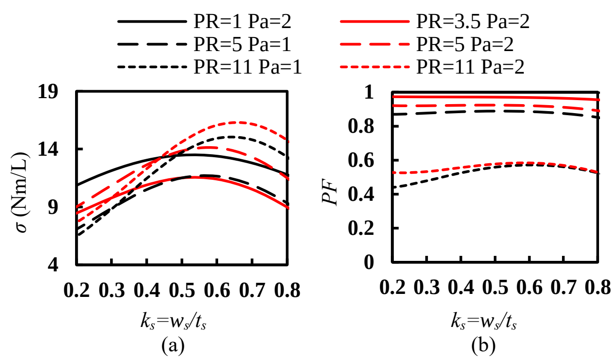

Fig. 5. The influence of stator slot opening width to slot pitch ratio k_s. (a) Torque density σ. (b) Power factor PF.

TABLE II
DESIGN PARAMETERS OF ORIGINAL MODELS

Design Parameters	PR=1 P_a=2	PR=3.5 P_a=2	PR=5 P_a=1	PR=5 P_a=2	PR=11 P_a=1	PR=11 P_a=2
Stator slot number, Z_s	6	9	6	12	12	24
PM pole-pair number, P_r	2	7	5	10	11	22
Armature winding pole-pair number, P_a	2	2	1	2	1	2
The ratio of PM pole-pair to armature winding pole-pair, PR	1	3.5	5	5	11	11
Phase current RMS value, I (A)	11.3	10.8	9.8	10.7	9.8	10.7
The ratio of total winding length to stack length l_{st}, k_{end}	1.03	1.13	1.28	1.15	1.28	1.15
The ratio of stator inner radius r_g to stator outer radius r_{so}, k_{split}	0.65	0.65	0.6	0.65	0.6	0.65
The ratio of slot depth l_t to stator depth ($r_{so}-r_g$), k_t	0.57	0.57	0.5	0.57	0.5	0.57
Stator inner radius, r_g (mm)	32.5	32.5	30	32.5	30	32.5
Stator outer radius, r_{so} (mm)	50					
Air-gap length, g (mm)	0.8					
Stack length, l_{st} (mm)	400					
PM remanence, B_r (T)	1.24					
Stator slot depth, l_t (mm)	10					
PM pole-arc, α_m	1					
Copper loss per-unit volume, k_{Copper} (kW/m^3)	76					
Slot filling factor, k_f	0.4					
Series turns per phase, N_s	60					
Rotor mechanical angular speed, Ω (r/min)	300					

This article has been accepted for publication in IEEE Transactions on Industry Applications. This is the author's version which has not been fully edited and content may change prior to final publication. Citation information: DOI 10.1109/TIA.2023.3245586

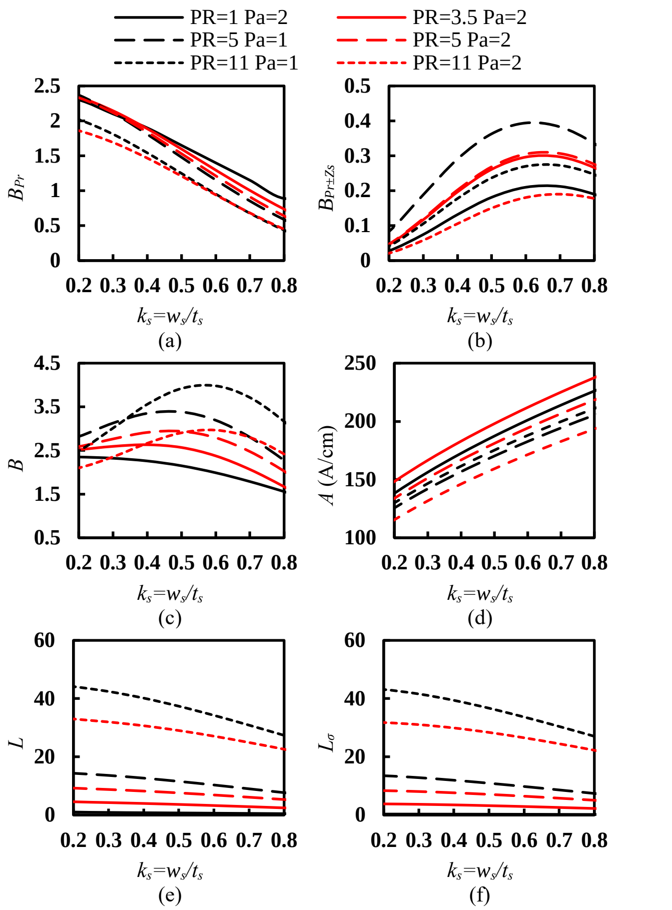

Fig. 6. The influence of stator slot opening width to slot pitch ratio k_s. (a) Air-gap harmonic B_{Pr}. (b) Air-gap harmonic $B_{Pr\pm Zs}$. (c) Magnetic loading B. (d) Electric loading A. (e) Inductance L. (f) Harmonic leakage L_σ.

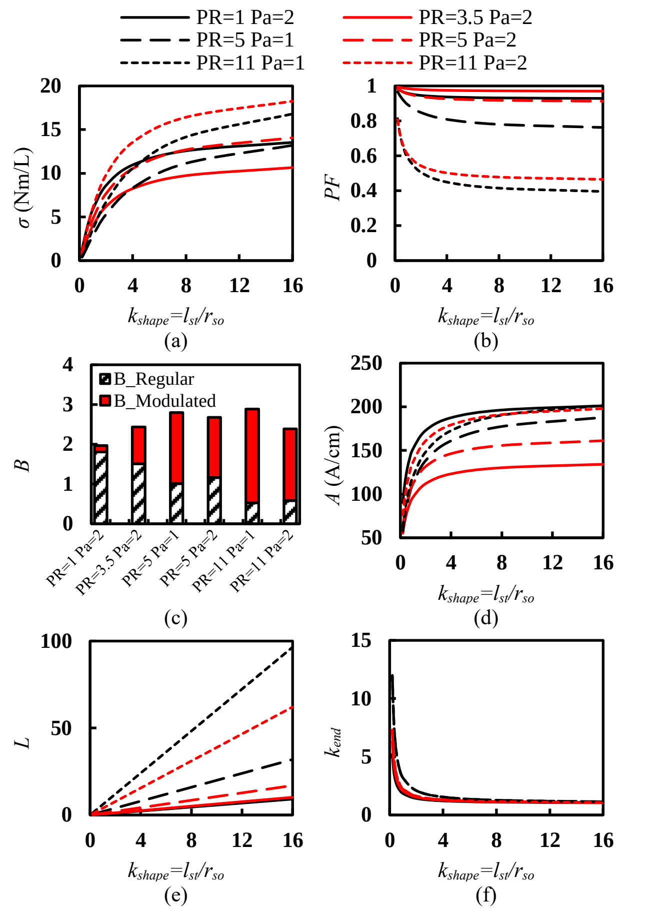

Fig. 7. The influence of pole-pair ratio PR covering different length-radius ratios k_{shape}. (a) Torque density σ. (b) Power factor PF. (c) Magnetic loading B. (d) Electric loading A. (e) Inductance L. (f) End-winding length factor k_{end}.

It can be observed in Fig. 7(a) that with the increase of k_{shape}, torque density σ is increased because of the negative influence of end-winding is weakened, while the electric loading A can be enhanced. The end-winding length factor k_{end} of SPMVMs with high PR is significantly higher than low PR counterparts, especially under small k_{shape} condition. As a result, compared to high PR SPMVMs, conventional PMSMs with fractional slot concentrated winding and low PR SPMVMs, can be up to the upper limit of torque density σ quickly. Moreover, the contributions of regular air-gap flux density harmonics B_{Pr} and modulated harmonics $B_{Pr\pm Zs}$ are compared, as depicted in Fig. 7(c). With the increase of PR, the effects of modulated harmonics $B_{Pr\pm Zs}$ on torque density σ are enhanced. Further, Fig. 7(b) shows that high PR SPMVMs suffer from low power factor, due to large inductance.

Thus, the selection of PR is strongly related to k_{shape}, which can be summarized that:

1) For torque density σ, the high PR SPMVMs are competitive when length-radius ratio $k_{shape} > 4$, where the negative effects of long end-winding can be neglected. However, with $k_{shape} \leq 4$, the regular fractional slot concentrated winding PMSMs and low PR SPMVM are attractive owing to the compact end-winding, as listed in Table II.

2) For power factor PF, the high PR SPMVMs suffer from low PF due to the abundant harmonic leakage inductances.

D.Armature Winding Pole-Pair P_a

It can be found that except the pole-pair PR, the effects of armature winding pole-pair P_a on torque density σ and power factor PF should also be taken into consideration. It can be found in Fig. 7 that under the same PR, the larger P_a, the lower magnetic loading B. The reason is that the air-gap fundamental relative permeance and flux modulation effects are weakened under the large P_a. However, the larger P_a is conductive to improve end-winding, electric loading A, and inductance L.

Therefore, the selection of P_a can be summarized as:

1) For torque density σ, the SPMVMs with large P_a are promising when length-radius ratio $k_{shape} > 4$, where the decrease of magnetic loading B can be compensated by the increase of electric loading A. However, with $k_{shape} \leq 4$, the SPMVMs with small P_a are attractive owing to the stronger flux modulation effects.

2) For power factor PF, the SPMVMs with large P_a is preferable due to decrease of inductance.

In a word, combined with the analysis mentioned above, how the parameters of SPMVMs affect torque density σ and power factor PF are summarized in Table III. Among which, the higher k_g, the higher PF due to the weakened inductance L under the large equivalent air-gap length. While with the increase of k_g, σ is increased first owing to the improvement of regular air-gap flux density harmonics, and then decreased due

This article has been accepted for publication in IEEE Transactions on Industry Applications. This is the author's version which has not been fully edited and content may change prior to final publication. Citation information: DOI 10.1109/TIA.2023.3245586

to the impairment of modulated air-gap flux density harmonics. For k_s, it is mainly related to σ, while the influence on *PF* can be neglected. The design of k_s should balance both the flux modulation effects and slot area, that is, achieve the relatively high magnetic loading *B* and electric loading *A* simultaneously. In terms of *PR*, the SPMVM with high *PR* can obtain the high *B* due to the strong flux modulation effect. Whereas it suffers from the low *PF* due to the large harmonic leakage inductance.

Moreover, the model with low armature winding pole-pair P_a and high *PR* suffer from the long end-winding length, which lead to the low electric loading *A*. As a result, the high torque density advantages of SPMVM with high *PR* can only be exploited under the large length-radius ratio k_{shape}. Further, the preferable selection ranges of critical parameters are determined, as listed in Table IV. It can be observed that with the increase of *PR*, the preferable k_g is decreased to enhance the flux modulation effects by decreasing equivalent air-gap length. While the preferable k_s is slightly increased to improve air-gap fundamental permeance, so as to have a better use of modulated air-gap flux density harmonics. Moreover, the high torque density advantages of SPMVMs with high *PR* can be performed under the relatively high k_{shape}.

TABLE III
INFLUENCE OF PARAMETERS ON MACHINE PERFORMANCES

Geometric Parameters	Electromagnetic Performance				
	B	*A*	*L*	σ	*PF*
k_g	↗↘	-	↘	↗↘	↗
k_s	↗↘	↗	↘	↗↘	–
PR	↗	↘	↗	↗↘	↘
P_a	↘	↗	↘	↗	↗
k_{shape}	-	↗	↗	↗	↘

where '↗↘', '↗', and '↘', represent increase first and then decline, monotonic increase, and monotonic decrease, respectively.

TABLE IV
PREFERABLE SELECTION RANGE OF NORMALIZED PARAMETERS

PR	Preferable k_g	Preferable k_s	Preferable k_{shape}
1	>6	<0.1	<0.5
2~3.5	4.5~5.5	0.2~0.35	0.5~1.5
3.5~5	3.5~4.5	0.35~0.55	1.5~2.5
5~8	3~3.5	0.55~0.6	2.5~4
>8	1~3	>0.6	>4

IV. GENERAL DESIGN APPROACH OF SPMVMS

Based on the relations between parameters and machine performances, as well as the preferable selection ranges of critical parameters, the general design approach of SPMVMs is proposed to balance torque density, power factor, and efficiency, covering different power ratings. And the detailed design flowchart is organized in Fig. 8.

Step 1: Determination of Initial Parameters

1) Based on the size of space, both the stator outer radius r_{so}, and the upper limit of length-radius ratio k_{shape} can be set.
2) According to power ratings and process craft, air-gap length *g* can be determined. Then, the air-gap length to stator outer radius ratio k_P can be calculated.
3) Combined with dissipation capability and machine efficiency requirements, the upper limit of copper loss factor k_{Copper} can be defined.
4) By materials characteristic, copper resistivity ρ and PM remanence B_r can also be acquired.
5) The upper limit of PM consumption can be determined based on cost.

Step 2: Design of Key Parameters

1) Based on the indexes of torque and power factor, the initial pole-pair ratio *PR* can be set.
2) Combined with k_{shape} and efficiency requirements, the armature winding pole-pair P_a can be selected.
3) According to the selected *PR*, the preferable stator slot opening width ratio k_s and magnet thickness to air-gap length ratio k_g can be determined.

Step 3: Design of Detailed Size

1) Based on the selected P_a and overloading capability requirements, the initial split ratio k_{split} and slot depth ratio k_t can be set.

Step 4: Evaluation of Performance

1) Based on the acquired parameters, initial model can be constructed, and the performance can be evaluated by FEA.
2) If all the performance are satisfied, flowchart can be completed. Otherwise, some iterations are needed.
3) If torque *T* is unsatisfied, P_a can be decreased to enhance flux modulation effects and magnetic loading *B*. Moreover, k_{split} can be increased to enhance air-gap radius.
4) If power factor *PF* is unsatisfied, inductance can be decreased by applying lower *PR* or larger P_a.
5) If efficiency η is unsatisfied, copper losses can be reduced by increasing P_a or decreasing *PR* to reduce end-winding.
6) If all the performance are unsatisfied, *PR* should be redefined.

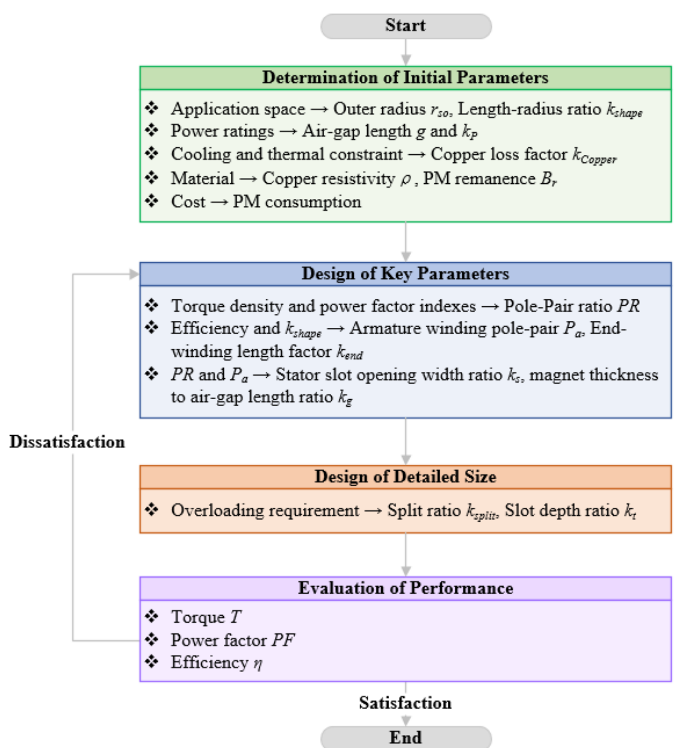

Fig. 8. The general design flowchart of SPMVMs.

This article has been accepted for publication in IEEE Transactions on Industry Applications. This is the author's version which has not been fully edited and content may change prior to final publication. Citation information: DOI 10.1109/TIA.2023.3245586

V. Design Examples and FEA Validations

In order to validate the analysis, two SPMVM examples named as Model 1 and Model 2 have been built based on the proposed design approach. Technical indexes and initial parameters are listed in Table V.

First, according to size upper limit, the initial k_{shape} can be determined. Further, based on rated power and speed, the targeted torque density σ can be predicted. Then, combined with torque density and power factor indexes, as well as the relation between pole-pair ratio PR and machine performance, the initial PR can be selected. In the design examples, the PR of Model 1 is selected as 3.5 to acquire high power factor PF, while the PR Model 2 is set as 14 to achieve high efficiency.

Further, based on the preferable selection range, the critical parameters, covering magnet thickness to air-gap length ratio k_g and stator slot opening width ratio k_s can be derived. In particular, the selection of k_g should also meet magnet consumption limit. Model 2 with high PR has the smaller k_g and larger k_s to strengthen the flux modulation effects. Next, based on the overloading requirements, slot depth ratio k_t and split ratio k_{split} can be determined, where Model 2 with high PR and low armature winding pole-pair P_a is easier to get saturated. Thus, the split ratio of which is smaller than Model 1.

TABLE V
Initial Parameters and Technical Indexes

Parameters	Values	Parameters	Values
Stator outer radius, r_{so}	< 167 mm	Stack length, l_{st}	< 50 mm
Air-gap length, g	0.7 mm	PM remanence, B_r	1.24 T
PM consumption	< 0.5 kg	Slot filling factor, k_f	0.4
Rated power, P	600 W	Overload capacity	1.5 times
Rated speed, ω	300 r/min	Power factor, PF	> 0.8
Copper resistivity, ρ	$2.17{*}10^{-4}$ $\Omega{*}m^2/m$	Efficiency, η	≥ 85%

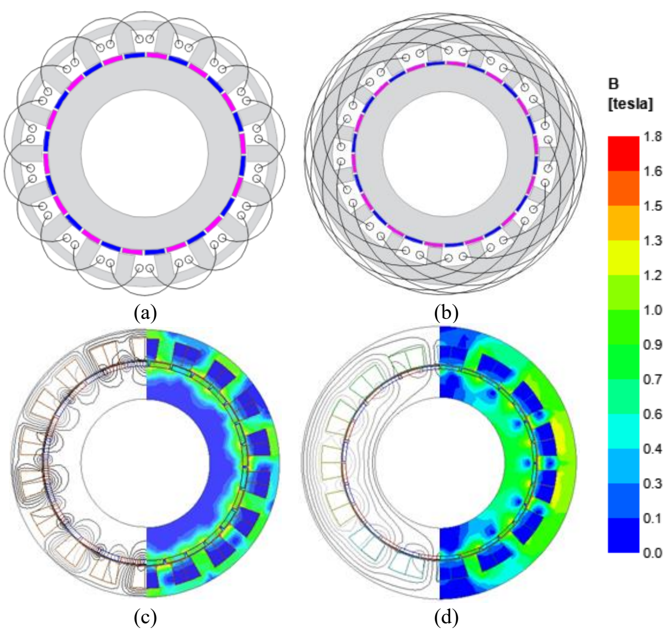

Fig. 9. The topology structure and no-load flux density distribution of two examples. (a) Structure of Model 1. (b) Structure of Model 2. (c) Flux density of Model 1. (d) Flux density of Model 2.

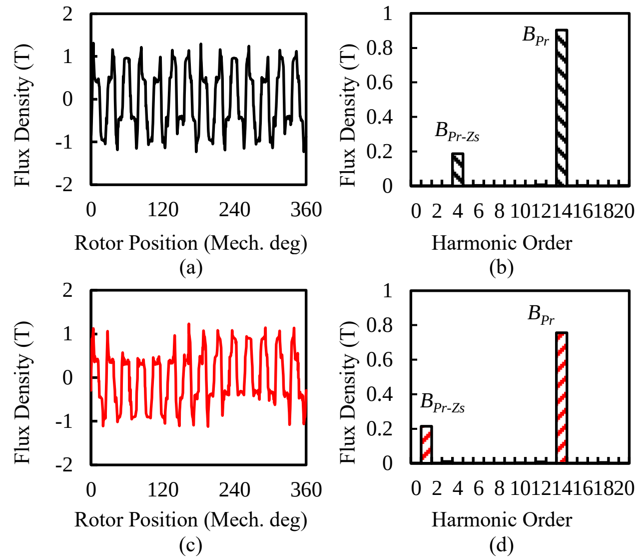

Fig. 10. No-load air-gap flux density of two models. (a) Waveforms of Model 1. (b) Spectrums of Model 1. (c) Waveforms of Model 2. (d) Spectrums of Model 2.

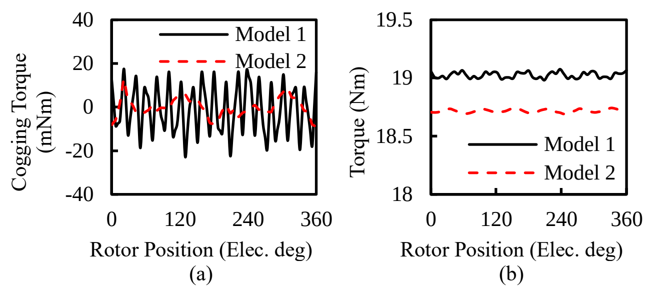

Fig. 11. Comparison of the torque waveforms for the two models. (a) Cogging torque. (b) On-load torque.

Fig. 9 shows machine structure and no-load flux density of two design examples. Fig. 10 presents the no-load air-gap flux density waveforms and spectrums of the two models. It can be seen that except for the regular air-gap flux density harmonics with the same pole-pair of PMs, the modulated air-gap flux density harmonics having the same pole-pair of armature winding are also generated.

Moreover, the torque waveforms of the two models are compared in Fig. 11. It can be observed in Fig. 11(a) that the cogging torques of the two models are low, where the peak-to-peak values are lower than 50 mNm. In particular, the Model 2 with high PR presents the lower cogging torque due to the strong flux modulation effects [22]. Fig. 11(b) shows the on-load toque waveforms, where the torque ripples of the two models are also low.

The detailed parameters and performances of two models are concluded in Table VI, where the analysis results match well with finite element analysis (FEA), which verify the feasibility of the proposed design and analysis. Both Model 1 and Model 2 can achieve targeted power and torque within the limit of machine size, power factor, efficiency and PM consumption. It can be noticed that benefited from high PR, Model 2 has higher magnetic loading B, which is 2.7 times to Model 1. As a result, Model 2 can achieve targeted power with lower electric loading A and higher efficiency η, although it suffers from the longer

This article has been accepted for publication in IEEE Transactions on Industry Applications. This is the author's version which has not been fully edited and content may change prior to final publication. Citation information: DOI 10.1109/TIA.2023.3245586

TABLE VI
PARAMETER AND PERFORMANCE COMPARISONS OF MODEL 1 AND MODEL 2

Parameters	Model 1			Model 2		
Slot-Pole combination $Z_s/P_r/P_a$	18/14/4			15/14/1		
Pole-Pair ratio PR	3.5			14		
Winding factor k_w	0.945			0.951		
Copper loss factor k_{Copper}, kW/m^3	76.4			34.5		
End-winding length factor k_{end}	2			4.9		
Stack length to stator outer radius ratio k_{shape}	0.6			0.6		
Air-gap length to stator outer radius k_P	0.8%			0.8%		
Magnet thickness to air-gap length ratio k_g	4.3			3.0		
Slot opening width to slot pitch ratio k_s	0.55			0.65		
Magnet consumption, kg	0.39			0.26		
Split ratio k_{split}	0.77			0.72		
Slot depth ratio k_t	0.71			0.5		
Performances	Analysis	FEA	Error	Analysis	FEA	Error
Magnetic loading B, T	2.43	2.4	0.3%	6.5	6.4	0.6%
Electric loading A, A/cm	172.5	-	-	73.2	-	-
Total inductance L, mH	3.3	3.2	3.1%	41	40	2.5%
Phase resistance R, Ω	0.7	-	-	1.9	-	-
Back EMF E, V	44.3	44.2	0.2%	111	107.8	2.8%
Torque T, Nm	19.1	18.9	1.1%	19.1	18.6	2.7%
Electromagnetic Power P, W	600	594	1.1%	600	584	2.7%
Effect volume torque density, Nm/L	17.4	17.2	1.1%	17.4	17	2.7%
Total volume torque density σ, Nm/L	8.8	8.7	1.1%	3.6	3.5	2.7%
Power factor PF	0.94	0.96	-2.1%	0.88	0.91	-3.3%
Copper losses P_{Copper}, W	84	-	-	38	-	-
Efficiency η, %	87.7	85.8	2.2%	94.0	92.8	1.3%

end-winding. Moreover, the power factor of Model 2 with high PR is inferior to Model 1, due to the larger inductance. It is worth noting that for the proposed Model 1 and 2, only the length-radius ratio $k_{shape} = 0.6$ is selected, which is based on the size upper limitation. For the conditions with k_{shape} higher than 0.6, the copper loss proportion of end-winding can be decreased, which is conducive to enhance the active electric loading A under the same total copper losses. In other words, to achieve the targeted torque, the copper losses caused by end-winding can be decreased and machine efficiency can be improved. As a result, the efficiency advantage of Model 2 with high PR=14 can be more significant.

VI. EXPERIMENTAL VALIDATIONS

In this section, two SPMVM prototypes of 18/14/4 (slot/PM-pole-pair/winding-pole-pair) and 15/14/1 with pole-pair ratio PR 3.5 and 14 are manufactured and tested to verify the analysis mentioned above. Fig. 12 performs the pictures of stator, surface-mounted PM rotor, winding, and test platform, respectively.

TABLE VII
PROTOTYPE PARAMETERS

Parameters	Values	Parameters	Values
Stack length	100 mm	Airgap length	0.7 mm
Stator outer diameter	167 mm	PM thickness	2.7 mm
Stator inner diameter	128 mm	Rotor pole-pair	14
Series turn per phase	180	Magnet material	N38UH
Rated speed	300 r/min	PM remanence, B_r	1.24 T
Rated Power	1 kW	Core material	50WW470

The main parameters and electromagnetic performances are listed in Table VII and VIII, where the two prototypes have the same stator outer diameter, stack length, and series turn per phase. And the same PM rotor has been used to save the manufacture cost.

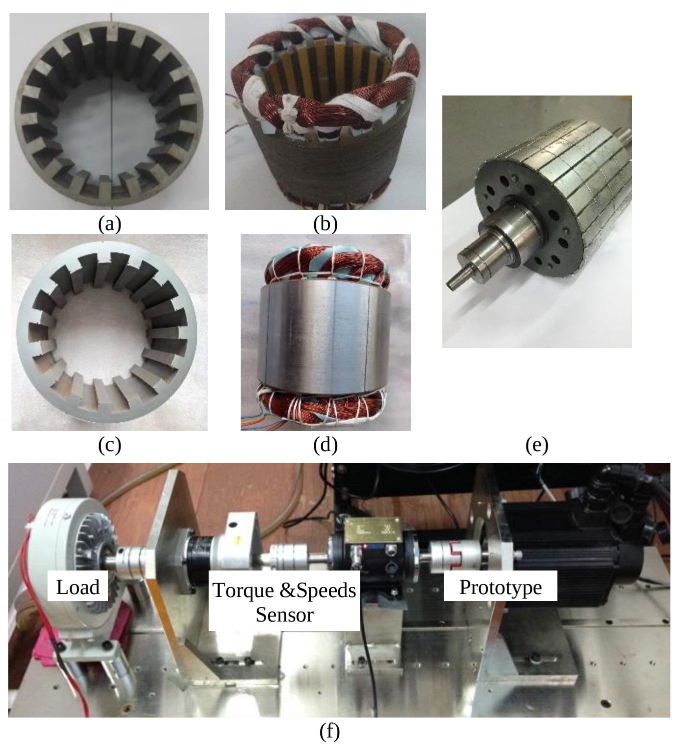

Fig. 12. Prototypes pictures. (a) 18-slot stator. (b) 4-pole-pair winding. (c) 15-slot stator. (d) 1-pole-pair winding. (e) Rotor. (f) Test bench.

This article has been accepted for publication in IEEE Transactions on Industry Applications. This is the author's version which has not been fully edited and content may change prior to final publication. Citation information: DOI 10.1109/TIA.2023.3245586

TABLE VIII
PROTOTYPE PERFORMANCES AT RATED POINT

Parameters	Prototype 18/14/4	Prototype 15/14/1
Torque, Nm	31.8	31.8
Current, A	5.4	2.1
Resistance, Ω	1	3.6
Self-Inductance, mH	7	59
Mutual-Inductance, mH	-2	-24
Power factor	0.95	0.86
Efficiency (Analysis)	92.2%	93.1%
Efficiency (FEA)	91.4%	92.3%
Efficiency (Measured)	89%	91%

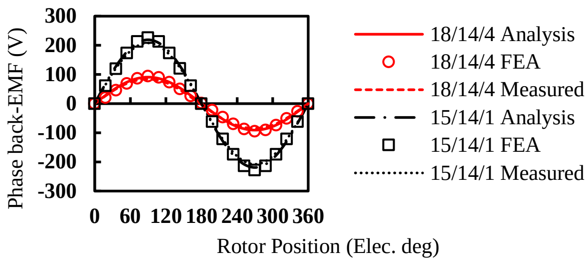

Fig. 13. Phase back-EMF waveforms at rotation speed 300 r/min.

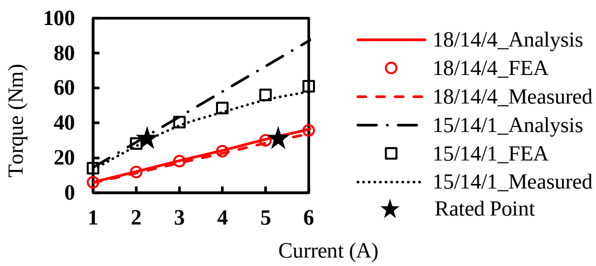

Fig. 14. Average torque versus phase current at rotation speed 300 r/min.

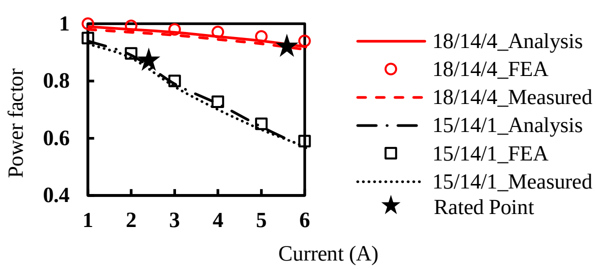

Fig. 15. Power factor versus phase current at rotation speed 300 r/min.

At first, the no-load performances of proposed SPMVMs are tested. Fig. 13 depicts the phase back-EMF waveforms at rotation speed 300 r/min, where the analysis, FEA and measured results have the good agreement. It can be seen that prototype 15/14/1 with high pole-pair ratio *PR* of 14 has the higher back-EMF due to the strong flux modulation effects and high magnetic loading, where the fundamental amplitudes are 218.3 V and 88.1 V, respectively. And the waveforms are sinusoidal.

Then, the on-load performances of proposed SPMVMs are further investigated. Considering winding inductance has small variation with the rotation of rotor, the conventional I_d = 0 control has been used. It can be seen in Fig. 14 that the prototype 15/14/1 with high *PR* 14 can achieve rated power with smaller rated current of 2.1 A, while the rated current of prototype 18/14/4 is up to 5.4 A. Although the resistance of prototype 15/14/1 is significantly higher than prototype 18/14/4 due to the long end-winding, the machine efficiency of prototype 15/14/1 is higher due to the smaller total copper losses produced by the low rated current. The machine efficiency of prototype 18/14/4 and prototype 15/14/1 at rated point are 89% and 91%, respectively. Moreover, it can be noticed that prototype 18/14/4 has the better torque linearity, where the torque is almost proportional to the current. However, prototype 15/14/1 with high *PR* suffers from large inductance caused by abundant armature harmonics, which is easier to get saturated.

Further, the power factor has been compared in Fig. 15, where prototype 18/14/4 can acquire the high power factor due to the small inductance. Whereas with the increase of current, the power factor of prototype 15/14/1 is quickly declined due to the large inductance. At rated condition, the power factor of prototype 18/14/4 and prototype 15/14/1 are 0.95 and 0.86, respectively.

Fig. 16 shows the measured torque, and phase current/voltage waveforms at the rated conditions. It can be seen that the torque ripples for the two prototypes are low. Moreover, it can be noticed that the phase angle difference between phase voltage and phase current of the prototype 18/14/4 is smaller than the prototype 15/14/1 counterpart due to the low inductance, which reflects the high power factor of SPMVMs with low *PR*.

Therefore, both the two prototypes can meet rated power, where the prototype 18/14/4 has the higher power factor, while the prototype 15/14/1 has the higher efficiency. Moreover, all the analysis, FEA, and measured results match well with each other, which confirmed the feasibility of the proposed analysis and design approach for SPMVM.

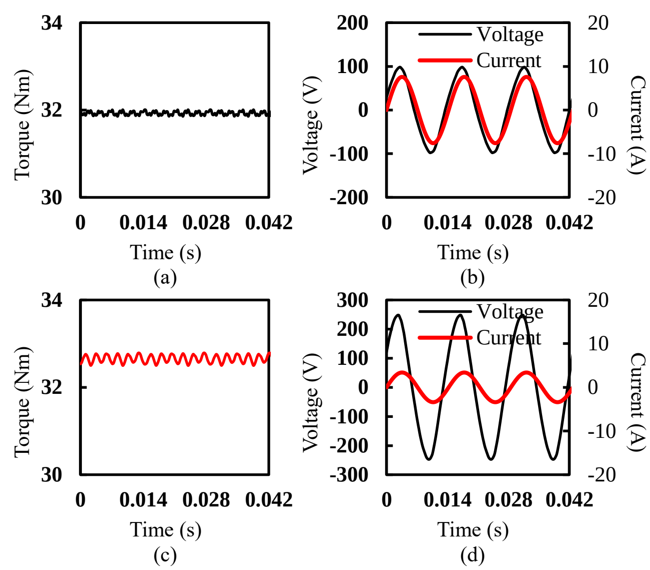

Fig. 16. Measured torque and phase voltage/current waveforms for the two models. (a) Torque of Model 1. (b) Phase voltage/current of Model 1. (c) Torque of Model 2. (d) Phase voltage/current of Model 2.

VII. CONCLUSIONS

This paper presents design considerations of SPMVMs to make a good compromise between machine performances. By means of closed-from per-unit equations, the negative correlation between torque density and power factor is revealed. Further, the cross-coupling influence of critical parameters, including magnet thickness to air-gap length ratio k_g, stator slot opening width to slot pitch ratio k_s, pole-pair ratio PR, armature winding pole-pair P_a, and length-radius ratio k_{shape}, on machine performances are clarified. Then, the preferable selection ranges are determined. In particular, the general design flowchart of SPMVMs is proposed, which can avoid the blind attempt and provide a good guidance for engineering designers.

The following conclusions are drawn:

1) When length-radius ratio k_{shape} larger than 4, SPMVMs with high pole-pair ratio PR are preferable due to the stronger flux modulation effects. However, benefited compact end-winding lengths, regular fractional slot concentrated winding PMSMs and low PR SPMVMs are attractive when k_{shape} smaller than 4.

2) Under the same PR and copper losses, the larger armature winding P_a is conducive to decrease end-winding length and inductance, so as to improve electric loading A and power factor PF. However, with k_{shape} smaller than 4, SPMVMs with smaller P_a are attractive due to the higher magnetic loading B.

3) The preferable magnet thickness to air-gap length ratio k_g of SPMVMs is lower than 6. With the increase of PR, the optimal k_g is decreased to strengthen flux modulation effects. However, the relatively large k_g is beneficial to weaken inductance.

4) The preferable stator slot opening width ratio k_s of SPMVMs is around 0.4~0.7. With the increase of PR, the optimal k_s is slightly enlarged to strengthen flux modulation effects.

Appendix

The coefficients of the air-gap relative permeance function can be figured out by conformal mapping method proposed in [2].

$$\Lambda_0 = 1 - 1.6\beta k_s \tag{15}$$

$$\Lambda_1 = \frac{4}{\pi}\beta\left(0.5 + \frac{k_s^{\,2}}{0.78125 - 2k_s^{\,2}}\right)\sin\left(1.6\pi k_s\right) \tag{16}$$

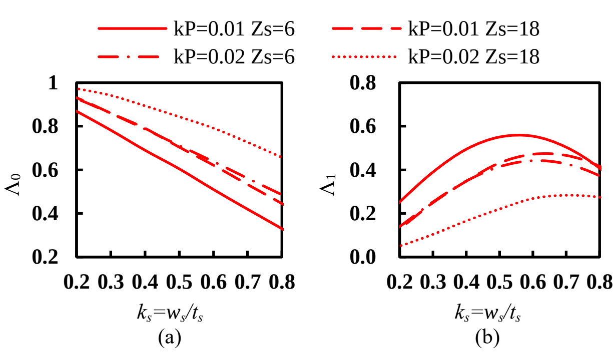

Fig. 17. Stator slot opening width ratio vs air-gap relative permeance covering different stator slot number Z_s and air-gap length to stator outer radius ratio k_P. (a) Λ_0. (b) Λ_1.

$$\beta = 0.5 - 1 \Big/ 2\sqrt{1 + \left(\frac{\pi k_{split} k_s}{k_P(1+PR)P_a(1+\frac{k_g}{\mu_r})}\right)^2} \tag{17}$$

$$k_s = \frac{w_s}{t_s},\ k_P = \frac{g}{r_{so}},\ k_{split} = \frac{r_g}{r_{so}} \tag{18}$$

$$Z_s = P_a + P_r = (1+PR)P_a \tag{19}$$

Fig. 17 presents the variation of air-gap relative permeance with k_s, under different stator slot number Z_s and air-gap length to stator outer radius ratio k_P. It can be seen that with the increase of k_s, the air-gap relative constant permeance Λ_0 is gradually decreased, while the air-gap relative fundamental permeance Λ_1 increases first and then decrease. The relatively large Λ_1 can be acquired with k_s around 0.4~0.7. Moreover, with the increase of stator slot number Z_s, Λ_0 can be increased, while Λ_1 is decreased, which means that under the same pole-pair ratio PR, the flux modulation effects would be impaired with large armature winding pole-pair P_a. Similarly, with the increase of air-gap length g and the ratio k_P, the flux modulation effects is deteriorated. In this paper, the air-gap length to stator outer radius ratio k_P is set as 0.1% for direct-drive application [23].

Acknowledgment

This work was supported by National Natural Science Foundation of China under Grant 51977094, Grant 52122705, and Grant 51991382.

References

[1] A. Toba and T. A. Lipo, “Generic torque-maximizing design methodology of surface permanent-magnet vernier machine,” *IEEE Trans. Ind. Appl.*, vol. 36, no. 6, pp. 1539-1546, Nov./Dec. 2000.

[2] B. Kim and T. A. Lipo, “Analysis of a PM vernier motor with spoke structure,” *IEEE Trans. Ind. Appl*., vol. 52, no. 1, pp. 217–225, Jan./Feb. 2016.

[3] D. Wu, et al, “Optimization Design of Power Factor for an In-Wheel Vernier PM Machine from the Perspective of Air-Gap Harmonic Modulation,” *IEEE Trans. Ind. Electron.*, vol. 68, no. 10, pp. 9265-9276, Oct. 2021.

[4] J. Bai, et al, “Characteristic Analysis and Verification of the Magnetic-Field-Modulated Brushless Double-Rotor Machine,” *IEEE Trans. Ind. Electron*., vol. 62, no. 7, pp. 4023-4033, July. 2015.

[5] J. Bai, J. Liu, et al, “Investigation of the Power Factor of Magnetic-Field Modulated Brushless Double-Rotor Machine,” *IEEE Trans. Power Electron.*, vol. 36, no. 1, pp. 423-432, Jan. 2021.

[6] L. Xu, G. Liu, W. Zhao, X. Yang, and R. Cheng, “Hybrid stator design of fault-tolerant permanent-magnet vernier machines for direct-drive applications,” *IEEE Trans. Ind. Electron.*, vol. 64, no. 1, pp. 179–190, Jan. 2017.

[7] T. J. Zou, et al, “Advanced high torque density PM Vernier machine with multiple working harmonics,” *IEEE Trans. Ind. Appl.*, vol. 53, no. 6, Nov./Dec. 2017.

[8] K. Xie, et al, “A Novel Permanent Magnet Vernier Machine with Halbach Array Magnets in Stator Slot Opening,” *IEEE Trans. Magn.*, vol. 53, no. 6, pp. 1-5, June 2017.

[9] Y. Gao, et al, “Comparative Analysis of Double Flux Modulation Permanent Magnet Machines with Different Stator PM Arrangements,” *IEEE Trans. Ind. Appl*., vol. 58, no. 2, pp. 1941-1951, Mar./Apr. 2022.

[10] W. Liu and T. A. Lipo, “Analysis of Consequent Pole Spoke Type Vernier Permanent Magnet Machine with Alternating Flux Barrier Design,” *IEEE Trans. Ind. Appl.*, vol. 54, no. 6, pp. 5918-5929, Nov./Dec. 2018.

[11] X. Ren, et al, “Investigation of Spoke Array Permanent Magnet Vernier Machine with Alternate Flux Bridges,” *IEEE Trans. Energy Convers.*, vol. 33, no. 4, pp. 2112-2121, Dec. 2018.

[12] D. Li, R. Qu, J. Li and W. Xu, “Consequent-Pole Toroidal-Winding Outer-Rotor Vernier Permanent-Magnet Machines,” *IEEE Trans. Ind. Appl.*, vol. 51, no. 6, pp. 4470-4481, Nov./Dec. 2015.

[13] K. Du, L. Xu, W. Zhao and G. Liu, “Analysis and Design of a Fault-Tolerant Permanent Magnet Vernier Machine with Improved Power Factor,” *IEEE Trans. Ind. Electron*., vol. 69, no. 5, pp. 4353-4363, May. 2022.

[14] D. Li, R. Qu and T. A. Lipo, “High-Power-Factor Vernier Permanent-Magnet Machines,” *IEEE Trans. Ind. Appl*., vol. 50, no. 6, pp. 3664-3674, Nov./Dec. 2014.

[15] Y. Gao, M. Doppelbauer, J. Ou and R. Qu, “Design of a Double-Side Flux Modulation Permanent Magnet Machine for Servo Application,” *IEEE J. Emerg. Sel. Topics Power Electron.*, vol. 10, no. 2, pp. 1671-1682, April. 2022.

[16] T. W. Ching, K. T. Chau and W. Li, “Power Factor Improvement of a Linear Vernier Permanent-Magnet Machine Using Auxiliary DC Field Excitation,” *IEEE Trans. Magn*., vol. 52, no. 7, pp. 1-4, July. 2016.

[17] Z. Q. Zhu and Y. Liu, “Analysis of Air-Gap Field Modulation and Magnetic Gearing Effect in Fractional-Slot Concentrated-Winding Permanent-Magnet Synchronous Machines,” *IEEE Trans. Ind. Electro.*, vol. 65, no. 5, pp. 3688-3698, May. 2018.

[18] Y. Liu, H. Y. Li and Z. Q. Zhu, “A High-Power Factor Vernier Machine with Coil Pitch of Two Slot Pitches,” *IEEE Trans. Mag.*, vol. 54, no. 11, pp. 1-5, Nov. 2018.

[19] T. Zou, et al, “Performance comparison of surface and Spoke-Type Flux-Modulation machines with different pole ratios,” *IEEE Trans. Magn*., vol. 53, no. 6, pp. 1–5, Jun. 2017.

[20] Y. Zhao, D. Li, X. Ren and R. Qu, “A General Design Approach of Surface-Mounted Permanent Magnet Vernier Machine,” International Power Electron. Conf., 2022, pp. 2167-2174.

[21] B. Boazzo, G. Pellegrino and A. Vagati, “Multipolar SPM Machines for Direct-Drive Application: A General Design Approach,” *IEEE Trans. Ind. Appl*., vol. 50, no. 1, pp. 327-337, Jan.-Feb. 2014.

[22] D. Li, R. Qu, J. Li, L. Xiao, L. Wu and W. Xu, “Analysis of Torque Capability and Quality in Vernier Permanent-Magnet Machines,” *IEEE Trans. Ind. Appl.*, vol. 52, no. 1, pp. 125-135, Jan.-Feb. 2016.

[23] A. B. Kjaer, S. Korsgaard, S. S. Nielsen, L. Demsa, and P. O. Rasmussen, “Design, fabrication, test, and benchmark of a magnetically geared permanent magnet generator for wind power generation,” *IEEE Trans. Energy Convers.*, vol. 35, no. 1, pp. 24–32, Mar. 2020.

Yu Zhao (Student Member, IEEE) was born in China. She received the B.E.E. degree in electrical engineering from Southwest Jiaotong University, Chengdu, China, in 2017. She is currently working toward the Ph.D. degree in electrical engineering at Huazhong University of Science and Technology, Wuhan, China. Her research interests include design and analysis of flux-modulation permanent-magnet machines.

Dawei Li (Senior Member, IEEE) was born in China. He received the B.E.E. degrees in electrical engineering from Harbin Institute of Technology, Harbin, China, in 2010 and the Ph.D. degree in electrical engineering from Huazhong University of Science & Technology, in 2015. In Jul. 2015, he joined Huazhong University of Science &Technology, Wuhan, China. Dr. Li has authored over 60 published technical papers and is the holder of over 10 patents/patent applications. He was recipient of the Best Poster Presentation Award from the XXII th International Conference on Electrical Machines (ICEM 2016), and Hubei Province Excellent Doctoral Dissertation (2016), China. His research areas include the design and analysis of flux-modulation permanent-magnet machines.

Xiang Ren was born in Hunan, China. He received the B.Eng. and Ph.D. degrees in electrical engineering from the Huazhong University of Science and Technology, Wuhan, China, in 2014 and 2019, respectively. He is currently a Postdoc with the Huazhong University of Science and Technology. His research interests include design and analysis of flux modulation machines.

Tianjie Zou (Member, IEEE) was born in Hubei, China, in 1991. He received the B.Sc. degree in electrical and electronic engineering and the Ph.D. degree in electrical engineering from the Huazhong University of Science and Technology, Wuhan, China, in 2013 and 2018, respectively.

He joined the Power Electronics, Machines and Control (PEMC) Group, University of Nottingham, Nottingham, U.K., in 2018, as a Research Fellow. In 2020, he was awarded the Nottingham Research Fellowship and started his independent research career. His main research interests include the design, analysis, and intelligent control of permanent-magnet machines. Dr. Zou was a recipient of the Best Paper Award in the 22nd International Conference on Electrical Machines (ICEM 2016).

Ronghai Qu (Fellow, IEEE) was born in China. He received the B.E.E. and M.S.E.E. degrees from Tsinghua University, Beijing, China, in 1993 and 1996, respectively, and the Ph.D. degree from the University of Wisconsin Madison, Madison, WI, USA, in 2002, all in electrical engineering.

In 1998, he joined the Wisconsin Electric Machines and Power Electronics Consortiums, University of Wisconsin–Madison, as a Research Assistant. In 2002, he became a Senior Electrical Engineer with Northland, a Scott Fetzer Company, Watertown, NY, USA. Since 2003, he has been with the Electrical Machines and Drives Laboratory, General Electric (GE) Global Research Center, Niskayuna, NY, USA, as a Senior Electrical Engineer. Since 2010, he has been a Professor with Huazhong University of Science and Technology, Wuhan, China. He has authored more than 230 published technical papers and is the holder of more than 50 patents/patent applications.